Evidence for enhanced convection of North Pacific Intermediate Water to the low-latitude Pacific under glacial conditions

L. Max[1*], N. Rippert[1], L. Lembke-Jene[1], A. Mackensen[1], D. Nürnberg[2], and R. Tiedemann[1]

[1]Alfred Wegener Institute, Helmholtz Centre for Polar and Marine Research, Bremerhaven, Am Alten Hafen 26, D-27568 Bremerhaven, Germany

[2]GEOMAR Helmholtz Centre for Ocean Research Kiel, Wischhofstr. 1-3, D-24148 Kiel, Germany

Corresponding author: Lars Max (Lars.Max@awi.de)

Key Points:

- Expansion of Glacial North Pacific Intermediate Water (GNPIW) to the tropical Pacific
- Glacial switch to additional influence of GNPIW at the Eastern Equatorial Pacific
- Enhanced GNPIW convection coincides with low-latitude nutrient- and marine productivity changes

Abstract

We provide high-resolution foraminiferal stable carbon isotope ($\delta^{13}C$) records from the subarctic Pacific and Eastern Equatorial Pacific (EEP) to investigate circulation dynamics between the extra-tropical and tropical North Pacific during the past 60 kyr. We measured the $\delta^{13}C$ composition of the epibenthic foraminiferal species *Cibicides lobatulus* from a shallow sediment core recovered from the western Bering Sea (SO201-2-101KL; 58°52.52'N, 170°41.45'E; 630 m water depth) to reconstruct past ventilation changes close to the source region of Glacial North Pacific Intermediate Water (GNPIW). Information regarding glacial changes in the $\delta^{13}C$ of sub-thermocline water masses in the EEP is derived from the deep-dwelling planktonic foraminifera *Globorotaloides hexagonus* at ODP Site 1240 (00°01.31'N, 82°27.76'W; 2921 m water depth). Apparent similarities in the long-term evolution of $\delta^{13}C$ between GNPIW, intermediate waters in the eastern tropical North Pacific and sub-thermocline water masses in the EEP suggest the expansion of relatively ^{13}C-depleted, nutrient-enriched, and northern-sourced intermediate waters to the equatorial Pacific under glacial conditions. Further, it appears that additional influence of GNPIW to the tropical Pacific is consistent with changes in nutrient distribution and biological productivity in surface-waters of the glacial EEP. Our findings highlight potential links between North Pacific mid-depth circulation changes, nutrient cycling, and biological productivity in the equatorial Pacific under glacial boundary conditions.

Keywords

North Pacific; Equatorial Pacific; stable isotopes; intermediate water; sub-thermocline; last glacial period

1 Introduction

The high latitudes of the North Pacific and the Southern Ocean play an essential role in regulating the exchange of CO_2 between the ocean and the atmosphere [*Takahashi et al.*, 2002]. In both regions, vertical mixing brings nutrient- and CO_2-rich deep waters into the euphotic zone and facilitates the biological pump, which sequesters atmospheric CO_2 back into the deeper ocean interior [e.g. *Honda et al.*, 2002]. In the modern North Pacific, however, the further exposure of nutrient- and CO_2-rich sub-surface waters to the surface ocean is largely hampered by a permanent halocline [*Haug et al.*, 1999]. In both regions, intermediate water masses are formed that re-circulate excess nutrients from the high-latitude oceans towards the low latitude-regions of the Pacific Ocean (Fig. 1). North Pacific Intermediate Water (NPIW) is formed in the sub-surface of the Northwest Pacific via mixing of high-nutrient sub-surface waters and intermediate water masses produced in coastal polynyas through brine rejection during wintertime sea-ice production in the Okhotsk Sea [*Talley*, 1993; *Shcherbina et al.*, 2003]. Today, NPIW circulates within the upper ~ 300 – 800 m and is mainly restricted to the subtropical North Pacific regions between ~ 20°N – 40°N, however a tongue of NPIW also spreads into the Celebes Sea in the western tropical Pacific [*Talley*, 1993; *Bostock et al.*, 2010]. In the Southern Ocean Antarctic Intermediate Water (AAIW) is produced at the surface ocean from upwelled nutrient- and CO_2-enriched Circumpolar Deep Water (CDW). AAIW further ventilates into the Subtropical Gyre and thereby transports heat, salt, and other chemical species, including dissolved CO_2, from the high latitudes of the Southern Ocean towards the equatorial Pacific. This, so-called “ocean tunnelling”, is one major process that provides nutrients to tropical Pacific thermocline waters today [e.g. *Bostock et al.*, 2010] (Fig. 1).

An important difference between northern- and southern-sourced intermediate waters is that sub-surface formation of NPIW largely prevents the biologically driven re-setting of deep ocean nutrient ratios that happens at the surface ocean during formation of AAIW. It is for this reason that NPIW is characterized by higher silicic acid to nitrate supply ratios compared to southern-sourced intermediate waters [*Sarmiento et al.*, 2004] (Fig. 1). On the other hand, as carbon fixation is dominated by siliceous phytoplankton at the surface-ocean near the formation region of modern AAIW, southern-sourced intermediate waters are characterized by high nitrate, but low silicic acid concentrations [*Sarmiento et al.*, 2004] (Fig. 1). Under modern conditions, mainly southern-sourced water masses (AAIW) are injected into the eastward-directed Equatorial Undercurrent (EUC) and the Equatorial Pacific Intermediate Water (EqPIW) via the South Equatorial Current and the New Guinea Coastal Undercurrent [*Dugdale et al.*, 2002]. The dominant role of AAIW on equatorial intermediate waters was also verified by a geochemical tracer analyses that suggests that EqPIW are primarily a combination of AAIW and Pacific Deep Water (PDW) with only a very minor contribution of NPIW today [*Bostock et al.*, 2010] (Fig. 1). As the intermediate water masses flow towards the east, they supply nutrients via diapycnal mixing to the overlying waters masses [*Rafter and Sigman*, 2016]. As a consequence of the high southern-sourced contribution today, carbon fixation by siliceous phytoplankton is limited by low silicic acid and iron availability in the Eastern Equatorial Pacific (EEP), making this region a significant net source of CO_2 to the atmosphere [*Dugdale et al.*, 2002].

Information regarding past deep ocean circulation changes can be reconstructed from the stable carbon isotopic composition ($\delta^{13}C$) measured on benthic foraminiferal tests. During the past

thirty years, this proxy has been successfully used to investigate glacial to interglacial changes in water mass geometry and ocean circulation [e.g. *Duplessy et al.*, 1984; *Curry et al.*, 1988; *Mix et al.*, 1991; *Curry et al.*, 2005; *Bostock et al.*, 2010; *Knudson and Ravelo*, 2015a]. In the modern ocean, high(low) values of $\delta^{13}C$ of the Dissolved Inorganic Carbon (DIC) are indicative of low(high) nutrient concentrations and large-scale oceanic water mass circulation patterns [*Kroopnick*, 1985]. For $\delta^{13}C$ reconstructions of intermediate- and deep-water mass circulation changes the initial $\delta^{13}C$, which is set in surface waters before subduction into the ocean interior, has to be taken into account. The initial $\delta^{13}C$ value of a water mass is affected by air-sea gas exchange at the surface-ocean, which in turn is temperature-dependent. After isolation from the surface-ocean, the $\delta^{13}C$ of a given water mass is mainly altered by in-situ addition of CO_2 through respiration of sinking organic material and mixing with other water masses. Today, a $\delta^{13}C_{DIC}$ of about 1 ‰ characterize surface waters of the North Atlantic where North Atlantic Deep Water (NADW) is formed. As it flows to the circum-Antarctic Ocean interior the continuous degradation of sinking organic particles reduces the original $\delta^{13}C_{DIC}$ of NADW to about 0.5 ‰. In the Southern Ocean deep-water further re-circulates to the Indian and Pacific Ocean and lowest values of ~ -0.6 ‰ $\delta^{13}C_{DIC}$ are observed today in the deep subarctic Pacific. Since $\delta^{13}C$ of epibenthic foraminifera is closely related to the $\delta^{13}C_{DIC}$ of ambient seawater, past differences in nutrient content and water mass circulation patterns can be reconstructed from benthic foraminiferal tests preserved in marine sediments [e.g. *Duplessy et al.*, 1984].

Combined evidence of $\Delta^{14}C$ deep-water ventilation ages and benthic foraminiferal $\delta^{13}C$ records suggest changes in mid-depth circulation (the upper 1000 to ~ 2000 m water depth) of the North Pacific Ocean under glacial conditions [*Duplessy et al.*, 1988; *Herguera et al.*, 1992; *Keigwin*,

1998; *Matsumoto et al.*, 2002a; *Okazaki et al.*, 2012]. Accordingly, the mid-depth circulation of the North Pacific was strengthened by formation of Glacial North Pacific Intermediate Water (GNPIW). In contrast to today, it has been proposed that the Bering Sea formed intermediate waters during glacial times and played an important role in formation of GNPIW [e.g. *Tanaka and Takahashi*, 2005; *Horikawa et al.*, 2010]. Evidence for additional cold and well-oxygenated intermediate water in the glacial Bering Sea has been provided from a study based on changes in radiolarian assemblages [*Tanaka and Takahashi*, 2005]. Based on a neodymium isotope record (εNd) it has been argued that Bering Sea intermediate water was a principal component of GNPIW during the glacial period [*Horikawa et al.*, 2010]. The formation of glacial Bering Sea intermediate waters was explained by changes in high-latitude hydrological processes such as enhanced brine rejection with the resulting salinity increase favouring the subduction of cold surface waters to the mid-depth in the Bering Sea as important precursor of GNPIW [*Rella et al.*, 2012]. A recent study based on endobenthic foraminiferal stable oxygen ($\delta^{18}O$) and $\delta^{13}C$ records from the Bering Sea indicates that enhanced GNPIW formation was not only restricted to the LGM, but also recurred during other extreme glacial intervals of the last 1.2 Myr [*Knudson and Ravelo*, 2015a].

There is so far no consensus about the amount of AAIW production during glacial boundary conditions. Based on $\delta^{13}C$ and $\delta^{18}O$ analyses on benthic foraminifera from the Australian margin it has been suggested that a colder and fresher water mass ventilated at intermediate depths, which was linked to a shift in the frontal zonation within the Southern Ocean [*Lynch-Stieglitz et al.*, 1994]. Furthermore, a study based on authigenic minerals from the Chilean margin found higher oxygen concentrations during glacial times, which were linked to an enhanced production

131 of AAIW [*Muratli et al.*, 2010]. In contrast, it has been proposed that stronger water column
132 stratification in the Southern Ocean led to a reduced production of AAIW under glacial
133 conditions [*Pahnke and Zahn*, 2005]. Accordingly, periods of increased intermediate water
134 formation were linked to Southern Hemisphere warm episodes through a tight coupling between
135 climate warming and intermediate water production at the high southern latitudes. A recent study
136 combined benthic $\delta^{13}C$ and $\delta^{18}O$ records off New Zealand with modelling results to reconstruct
137 the vertical extent of AAIW over the last 350 kyr [*Ronge et al.*, 2015]. These results showed that
138 the vertical extent of AAIW changed on glacial-interglacial timescales with a significantly
139 shallower AAIW subduction under glacial conditions. The shallower subduction of glacial
140 AAIW has been related to an advanced winter sea-ice edge as well as enhanced freshwater flux
141 from sea-ice melting, which reduced the salinity and resulted in formation of less dense
142 intermediate waters in the Southern Ocean.
143
144 Studies based on εNd records as well as $\Delta^{14}C$ shallow- and deep-water ventilation ages from the
145 equatorial Pacific suggest a dominant role of the Southern Ocean in transferring climatic signals
146 from the high latitudes towards the tropical regions during late Marine Isotope Stage (MIS) 2
147 [*Pena et al.*, 2013; *de la Fuente et al.*, 2015]. Accordingly, available reconstructions of changes
148 in water mass signatures of the equatorial Pacific suggest a principal southern-source for tropical
149 Pacific intermediate water masses during glacial times similar to today. In a recent study,
150 *Carriquiry et al.* [2015] analysed $\delta^{13}C$ records at the western Baja California Margin and relates
151 changes in mid-depth nutrient distribution to a larger influence of glacial AAIW to the tropical
152 North Pacific. In contrast, *Leduc et al.* [2010] explained anomalies in glacial $\delta^{13}C$ of
153 intermediate waters in the Eastern Tropical North Pacific (ETNP) by a switch from southern

154 nutrient-poor to northern nutrient-enriched intermediate water masses due to a sustained
155 formation of GNPIW. This notion is supported by a recent εNd data compilation from 55 core
156 sites around the Pacific [*Hu et al.*, 2016] that revealed a significant offset in EEP εNd signature
157 values between LGM and Holocene values (by 1–2 epsilon units lower than during the
158 Holocene), which can only be explained by a higher contribution from northern-sourced waters
159 [*Hu et al.*, 2016]. The enhanced penetration of northern-sourced water masses is in agreement
160 with evidence for enhanced glacial mid-depth circulation reconstructed from $\delta^{13}C$ records of
161 California margin sediment cores, however these records also point to spatial and temporal
162 complexity in the ventilation history of the Northeast Pacific [*Stott et al.*, 2000]. Together, these
163 results imply a more prominent role of GNPIW in shaping the mid-depth water mass
164 characteristics of the glacial North Pacific. On the other hand, it still remains illusive how
165 strengthened GNPIW circulation shaped the mid-depth water mass characteristics of the glacial
166 North Pacific and whether GNPIW might have influenced the nutrient distribution, biological
167 productivity and export patterns far beyond the northern high latitudes.
168
169 In this study, we report on stable isotope measurements derived from sedimentary records of the
170 western subarctic Pacific (Bering Sea) and EEP to investigate spatiotemporal changes in GNPIW
171 circulation and its influence on low-latitude Pacific water mass characteristics during the past 60
172 kyr. We chose a sediment core from the western Bering Sea located on Shirshov Ridge (SO201-
173 2-101KL, 58°52.52'N, 170°41.45'E, 630 m water depth, Fig. 1) and measured the $\delta^{13}C$
174 composition of the epibenthic foraminifera *Cibicides lobatulus* (*C. lobatulus*) as an indicator for
175 past ventilation changes close to the source-region of GNPIW [*Max et al.*, 2014]. Today the
176 western Bering Sea is poorly ventilated due to the absence of local intermediate water formation

177 and water masses bathing core site SO201-2-101KL are dominated by upwelling of nutrient-rich
178 PDW (Fig. 1b). Additional $\delta^{13}C$ data of deep-dwelling planktonic foraminifera *Globorotaloides*
179 *hexagonus* (*G. hexagonus*) from Ocean Drilling Program (ODP) Site 1240 (00°01.31'N,
180 82°27.76'W, 2921 m water depth, Fig. 1) provide information about glacial changes of sub-
181 thermocline water mass characteristics in the EEP. Modern water mass signatures of sub-
182 thermocline waters at ODP Site 1240 are linked to the lower branch of the EUC, which brings
183 nutrients to the surface ocean of the EEP (Fig. 1b). By comparing water mass signatures of
184 intermediate- to deep-water masses of the Pacific Ocean and Southern Ocean with sub-
185 thermocline to mid-depth water masses in the tropical Pacific we examine whether (1) the
186 influence of northern-sourced versus southern-sourced water masses on tropical Pacific
187 intermediate- and sub-thermocline water masses of the EEP changed during the last glacial
188 period and (2) discuss potential implications for sub-thermocline nutrient availability and
189 biological productivity in the equatorial Pacific in the past.

190

191 **2 Materials and Methods**

192 2.1. Stable carbon ($\delta^{13}C$) and oxygen ($\delta^{18}O$) isotope measurements from benthic and deep-
193 dwelling planktonic foraminifera

194 We measured the $\delta^{13}C$ and $\delta^{18}O$ isotope composition of epibenthic foraminifera *C. lobatulus*
195 selected from sediment samples of western Bering Sea sediment core SO201-2-101KL and deep-
196 dwelling planktonic foraminifera *G. hexagonus* from samples of ODP Site 1240 in the Panama
197 Basin (Fig 1; see supplementary Table S1 and S2). Sedimentation rates of 11 – 16 cm kyr^{-1} have
198 been reported for core SO201-2-101KL from Shirshov Ridge [*Riethdorf et al.*, 2013] and 6.4 –

199 25.2 cm kyr^{-1} for ODP Site 1240 [*Pena et al.*, 2008]. According to our sampling scheme we
200 achieved a millennial to centennial-scale resolution of proxy-data in this study with an average
201 temporal resolution of ~ 0.25 kyr for core SO201-2-101KL and ~ 0.23 kyr for the last 60 kyr of
202 ODP Site 1240, respectively. Stable isotope analyses in core SO201-2-101KL were made on
203 samples of two to three specimens of *C. lobatulus* picked from the 250 – 400 µm size fractions.
204 The stable isotopic composition of *G. hexagonus* of ODP Site 1240 were determined using five
205 specimens per sample picked from the 250 – 315 µm size fraction.
206
207 It has been proposed that *C. lobatulus* preferentially lives attached to hard substrate on or slightly
208 above the sediment surface and studies on living specimen indicated that this species faithfully
209 records the $\delta^{13}C_{DIC}$ of ambient seawater [*Schweizer et al.*, 2009]. Some investigators have
210 observed a positive offset in the $\delta^{13}C$ of *C. lobatulus* with regard to ambient bottom water
211 $\delta^{13}C_{DIC}$ in some high-latitude settings of the North Atlantic Ocean [*Mackensen et al.*, 2000].
212 However, this effect was caused by high seasonal variability of the original ambient $\delta^{13}C_{DIC}$-
213 signal, confirmed by time-series measurements of water column $\delta^{13}C_{DIC}$ and related to the
214 calcification of *C. lobatulus* during time intervals of maximum ventilation [*Mackensen et al.*,
215 2000]. We thus regard the $\delta^{13}C$-signal *C. lobatulus* to reliably reflect $\delta^{13}C$ of ambient seawater.
216
217 Isotopic compositions of *C. lobatulus* and *G. hexagonus* were measured at the Alfred Wegener
218 Institute, Helmholtz Centre for Polar and Marine Research, Germany, using a Thermo Fisher
219 MAT 253 mass spectrometer coupled to a Kiel IV automatic carbonate preparation device. All
220 stable isotope measurements were calibrated via the NBS-19 international standard and results
221 are reported in δ-notation versus VPDB scale. Overall long-term analytical reproducibility of

222 measurements based on internal laboratory standard (Solnhofen limestone) together with
223 samples over a one-year period is better than ±0.06 ‰ for $\delta^{13}C$ and ±0.08 ‰ for $\delta^{18}O$.
224
225 2.2. Stable oxygen isotope composition ($\delta^{18}O$) and apparent calcification depth of deep-
226 dwelling planktonic foraminifera *G. hexagonus*
227 Information regarding apparent calcification depth (ACD) of the planktonic foraminifera
228 *G. hexagonus* is still sparse. We make a first attempt to determine the ACD at ODP Site 1240 to
229 validate the depth habitat of *G. hexagonus* in the EEP. The ACD-estimation was done by
230 comparing measured foraminiferal $\delta^{18}O_{calcite}$ from a near core-top sample (at 10 cm) to a
231 theoretically expected equilibrium $\delta^{18}O$ values of calcite ($\delta^{18}O_{equilibrium}$) that foraminifera would
232 incorporate in dependence of modern water temperature, salinity and $\delta^{18}O$ values of seawater
233 ($\delta^{18}O_{seawater}$). In order to calculate $\delta^{18}O_{seawater}$, the $\delta^{18}O_{seawater}$-salinity relationships given by *Leduc*
234 *et al.* [2007] for 0–40 m water depth:
235
236 $\delta^{18}O_{seawater}$ (‰) = 0.253*S-8.52,
237
238 and for >40 m water depth:
239
240 $\delta^{18}O_{seawater}$ (‰) = 0.471*S-16.15
241
242 were used in conjunction with annual salinity data derived from World Ocean Atlas 2009
243 [*Antonov et al.*, 2010].
244

Several established $\delta^{18}O$-paleotemperature equations [*Epstein et al.*, 1953; *Shackleton*, 1974; *Kim and O'Neil*, 1997; *Bemis et al.*, 1998] were considered for $\delta^{18}O_{calcite}$ as absolute ACD estimation strongly depends on the applied temperature equation [*Wejnert et al.*, 2013] (Fig. 2). Modern temperatures are derived from the World Ocean Atlas 2009 [*Locarnini et al.*, 2010], and $\delta^{18}O_{seawater}$ were included after correcting $\delta^{18}O_{seawater}$ to the VPDB scale by subtracting the $\delta^{18}O_{seawater}$-conversion factor given in *Bemis et al.* [1998]. The water depth showing the best match between $\delta^{18}O_{calcite}$ and $\delta^{18}O_{equilibrium}$ is taken as the ACD of *G. hexagonus* (Fig. 2).

The calculated ACD suggests that *G. hexagonus* dwells below the thermocline in 340 – 430 m water depth similar to estimated depth habitats defined by *Ortiz et al.* [1996] in the North Pacific. Further support comes from a very recent ACD assessment from the western equatorial Pacific, which concludes that deep-dwelling *G. hexagonus* is a suitable proxy for tracing properties of equatorial sub-thermocline water masses [*Rippert et al.*, 2016]. Hence, the stable isotopic composition of *G. hexagonus* is considered to reflect the water mass properties of sub-thermocline waters of the EEP.

2.3. Stratigraphic approach and age models

The stratigraphic framework of western Bering Sea core SO201-2-101KL was constructed using a multi-proxy approach described in detail in *Riethdorf et al.* [2013]. Briefly, information derived from high-resolution X-ray fluorescence (XRF) and spectrophotometric logging data (color b*) of core SO201-2-101KL were used for correlation to millennial-scale variability preserved in the NGRIP ice core [*Andersen et al.*, 2004] according to the GICC05 timescale [*Svensson et al.*, 2008] (Fig. 3a). The tuning of core SO201-2-101KL to NGRIP was further

validated by five planktonic radiocarbon ages spanning the time interval from the onset of MIS 2 to the time interval of the last glacial termination (Fig. 3a) [see *Max et al.*, 2012].

We adopted the established age scale of ODP Site 1240 described in the work of *Pena et al.* [2008]. The stratigraphic framework of ODP Site 1240 was constructed from 17 AMS ^{14}C ages based on monospecific samples of the planktonic foraminifera *Neogloboquadrina dutertrei* (*N. duterteri*) and tuning of the initiation of *N. duterteri* $\delta^{13}C$ minima at ODP Site 1240 to the CO_2 increase in the Vostok CO_2, as shown by *Spero and Lea*, [2002]. Graphical correlation of planktonic foraminiferal Mg/Ca derived sea surface temperatures (SST) from ODP Site 1240 to Antarctic Vostok deuterium records was used to get additional age controls for deeper parts of the core [see supplement of *Pena et al.*, 2008 for more details] (Fig. 3b).

3 Results

The reconstructed glacial (60 – 20 ka) $\delta^{13}C$ values based on *C. lobatulus* from Bering Sea core SO201-2-101KL show a pronounced variability on millennial timescales, in particular during MIS 3, where they vary between -0.8 – 0.2 ‰ (Fig. 4). Upon millennial-scale variability a long-term trend towards increased $\delta^{13}C$ of Bering Sea intermediate water since the beginning of MIS 3 is clearly visible in core SO201-2-101KL, which culminated during early MIS 2 (~ 29 ka) with $\delta^{13}C$ signatures of up to ~ 0.3 ‰ (Fig. 4). During MIS 2 $\delta^{13}C$ values show a long-term decrease with $\delta^{13}C$ signatures reaching ~ -0.2 ‰ at the beginning of the last deglaciation (~ 17 ka).

During MIS 3 (~ 60 – 30 ka) the *G. hexagonus* $\delta^{13}C$ proxy record from ODP Site 1240 indicates the presence of relatively ^{13}C-enriched (nutrient-depleted) water masses with $\delta^{13}C$ signatures of

291 0.1 – 0.2 ‰ and relatively low variability in $\delta^{13}C$ of sub-thermocline waters (Fig. 4). A first
292 switch to relatively ^{13}C-depleted sub-thermocline water masses in the EEP is apparent during
293 early MIS 2 (~ 25 ka), the most ^{13}C-depleted values of ~ -0.4 ‰ are found at the beginning of
294 the last deglaciation (~ 17 ka).

295

296 **4 Discussion**

297 Based on our results, we found evidence that the Bering Sea experienced a long-term increase in
298 intermediate water ventilation from the beginning of MIS 3. We also identified most enhanced
299 ventilation of the Bering Sea during MIS 2, which is in accordance with recent results from
300 Knudson and Ravelo [2015a]. In general, it confirms previous studies on marine productivity and
301 benthic foraminiferal stable isotope records that imply a long-term increase in $\delta^{13}C$ Bering Sea
302 intermediate water due to local formation of waters masses with lower salinity and higher
303 oxygen content under glacial conditions [*Schlung et al.*, 2013]. *Rella et al.* [2012] argued that an
304 eastward displacement of the Aleutian Low and a shift to predominantly northerly winds over the
305 Bering Sea created favourable conditions for active polynya formation and brine rejection
306 coupled to sea-ice formation, which led to intermediate water production as one potential source-
307 region of GNPIW during the glacial period. A recent study showed that during stadial periods of
308 the deglaciation most of the western Bering Sea was covered by seasonal sea ice [*Méheust et al.*,
309 2016], thus providing favourable conditions for intermediate water formation. Moreover, benthic
310 $\delta^{13}C$ data from proximal core SO201-2-85KL point to a decline in $\delta^{13}C$ and reduced ventilation
311 during deglacial warm stages and the early Holocene when sea-ice cover was substantially
312 reduced [*Max et al.*, 2012; *Max et al.*, 2014]. However, changes in thermodynamic (temperature-

dependent) equilibration between the surface ocean $\delta^{13}C_{DIC}$ and the atmospheric CO_2 also influence isotopic fractionation, whereby surface ocean $\delta^{13}C_{DIC}$ increases by 0.1 ‰ with each 1°C decrease in surface ocean temperature [*Mook* et al., 1974]. Given that glacial production of intermediate waters in the western Bering Sea was supposedly linked to sea-ice formation during winter, when surface ocean temperature were always close to the freezing point, temperature-dependent changes in air-sea gas exchange of western Bering Sea surface waters should have had a minor effect on the $\delta^{13}C_{DIC}$ signal.

4.1. Glacial contribution of northern- *versus* southern-sourced water masses in the Eastern Tropical North Pacific (~ 8°N)

To assess the influence of northern- versus southern-sourced water masses on EqPIW characteristics during the past 60 kyr we compare benthic $\delta^{13}C$ mid-depth records from the subarctic Pacific (SO201-2-101KL; this study) and the Southern Ocean (SO213-84-1; *Ronge et al.*, 2015) as well as a deep-water benthic $\delta^{13}C$ record from the Northeast Pacific (W8709A-13PC; *Lund and Mix,* 1998) with mid-depth $\delta^{13}C$ signatures derived from sediment core MD02-2529 [*Leduc et al.*, 2010] located in the ETNP (Fig. 1 and 5a). The core site of MD02-2529 in the ETNP is situated at the modern confluence of northern oxygen-poor and southern oxygen-rich waters, and thus is ideally located to investigate past changes in the respective latitudinal extents of northern versus southern-sourced water masses in the past [*Leduc et al.*, 2010].

First, we consider our new benthic $\delta^{13}C$ record from the mid-depth subarctic Pacific (SO201-2-101KL) and the benthic $\delta^{13}C$ record of PDW from the Northeast Pacific (W8709A-13PC) [*Lund and Mix*, 1998], which are compared with EqPIW $\delta^{13}C$ water mass characteristics (MD02-2529)

[*Leduc et al.*, 2010] during the past 60 kyr (Fig. 1 and 5a). Millennial-scale variability superimposed on the long-term $\delta^{13}C$ trend of EqPIW is more pronounced compared to the $\delta^{13}C$-signal recorded in SO201-2-101KL (GNPIW) or W8709A-13PC (PDW) during early MIS 3 (55 – 45 ka). In addition EqPIW $\delta^{13}C$ values oscillate between $\delta^{13}C$ signatures of GNPIW and PDW during MIS 3 (60 – 30 ka). During this time, there is no clear relationship to northern- or southern-sourced intermediate waters, and rather admixing of different source water masses to EqPIW is likely. On the other hand, clear similarities in the long-term evolution in $\delta^{13}C$ between the intermediate water records derived from subarctic Pacific core SO201-2-101KL and sediment core MD02-2529 from the ETNP are observed since at least ~ 29 ka (Fig. 5a). Moreover, glacial gradients in $\delta^{13}C$ between GNPIW and EqPIW are relatively small and vary between 0.2 – 0.5 ‰. In contrast, absolute $\delta^{13}C$ signatures as well as the temporal evolution of EqPIW and PDW differs substantially such as $\delta^{13}C$ of EqPIW increases steadily, whereas $\delta^{13}C$ of PDW shows a long-term trend to more depleted ^{13}C signatures during MIS 2 (Fig. 5a). Accordingly, available deep-water ventilation ages as well as the long-term trend in deep-water $\delta^{13}C$ of the North Pacific indicate that glacial PDW was similar or even less well ventilated than today [*Lund and Mix*, 1998; *Galbraith et al.*, 2007; *Lund et al.*, 2011] and the ventilation history different to the mid-depth circulation dynamics of the North Pacific [*Kennett and Ingram*, 1995; *Stott et al.*, 2009]. Altogether, our results indicate that intermediate waters in the subarctic Pacific and ETNP (GNPIW and EqPIW) share similar glacial $\delta^{13}C$ signatures, which are indicative for the presence of nutrient-enriched intermediate water masses, but are apparently different to $\delta^{13}C$ signatures of PDW (Fig. 5a). Given that GNPIW features slightly higher $\delta^{13}C$ signatures compared to EqPIW masses our results point to the advection of northern-sourced intermediate water masses towards the tropical Pacific. Thus, from similarities in long-term

359 evolution of $\delta^{13}C$ between the North Pacific and ETNP intermediate water records we argue that
360 relatively nutrient-enriched GNPIW generally extended further south to the tropical Pacific
361 under glacial conditions. During the last deglaciation (~ 17 – 15 ka), however, intermediate
362 water $\delta^{13}C$-signals at the ETNP and North Pacific starts to diverge substantially. The $\delta^{13}C$
363 signatures in the ETNP increase, while the $\delta^{13}C$ values decrease at site SO201-2-85KL in the
364 subarctic Pacific (Fig. 5a).
365
366 The glacial $\delta^{13}C$ end-member variability of AAIW is reflected by sediment core SO213-84-1 off
367 New Zealand, where glacial $\delta^{13}C$ signatures of AAIW vary between ~ 0.5 – 1.4 ‰ [*Ronge et al.*,
368 2015] (Fig. 5a). The long-term evolution of $\delta^{13}C$-signatures between AAIW and intermediate
369 waters in the North Pacific and ETNP reveals remarkable differences in temporal variability
370 under glacial conditions (Fig. 5a). Moreover, huge gradients in $\delta^{13}C$ (up to 2 ‰) between
371 Southern Ocean core SO213-84-1 and MD02-2529 from the ETNP [*Leduc et al.*, 2010] clearly
372 separate ^{13}C-enriched (more nutrient-depleted) signatures of AAIW from ^{13}C-depleted (more
373 nutrient-enriched) signatures of EqPIW under glacial conditions (Fig. 5a). Evidence for a
374 weakened production or shoaling of glacial AAIW has been inferred from $\delta^{13}C$-records off New
375 Zealand [*Pahnke and Zahn*, 2005; *Ronge et al.*, 2015], which generally points to a glacial change
376 in relative contribution of intermediate waters from the Southern Ocean to the tropical Pacific.
377 Thus, large gradients and the discrepancy in temporal evolution of $\delta^{13}C$ signatures of EqPIW and
378 AAIW are indicative for additional water masses influencing the glacial mid-depth tropical
379 Pacific.
380

Independent evidence for enhanced glacial influence of northern-sourced intermediate waters to the low-latitude Pacific comes from the comparison of available εNd records of the Bering Sea and off Baja California [*Basak et al.*, 2010; *Horikawa et al.*, 2010] (Fig. 5b). In particular, εNd data at the intermediate depth in the Bering Sea show radiogenic values explicitly indicating that Bering Sea surface water masses (marked by more radiogenic εNd signatures) were subducted to intermediate depths under glacial conditions [*Horikawa et al.*, 2010]. At the same time, glacial εNd values derived from a sediment record off Baja California point to the presence of more radiogenic intermediate water masses, which has been linked to admixture of dominantly northern-sourced intermediate waters [*Basak et al.*, 2010]. Furthermore, available information of glacial εNd signatures from a sediment core in the Southwest Pacific [*Noble et al.*, 2013] clearly distinguish less radiogenic εNd signatures of AAIW from signals of more radiogenic intermediate water masses found in the Bering Sea or off Baja California (Fig. 5b). Altogether, results from εNd records are in line with enhanced glacial advection of northern-sourced intermediate water masses towards the tropical Pacific (Fig. 1 and 5b). However, rapid changes in Bering Sea and Baja California εNd signatures are visible during the last deglaciation that point to a switchback to reduced influence of northern-sourced intermediate water masses to the low-latitude Pacific since ~ 17 ka (Fig. 5b).

The combined evidences from $\delta^{13}C$ and εNd proxy data of the subarctic Pacific, the eastern North Pacific (Baja California), the ETNP and Southern Ocean suggest that northern-sourced intermediate waters extended further south to the ETNP under glacial conditions (Fig. 5a and b). This is in agreement with a scenario proposed by *Herguera et al.* [2010], in which a deepening of the main thermocline and cooling of the high-latitude North Pacific would lead to a south-

404 eastward expansion of GNPIW circulation and greater glacial influence of northern-sourced
405 intermediate water on the tropical Pacific. Therefore, we propose that glacial changes in the
406 relative contribution of intermediate waters from both the Southern Ocean and North Pacific are
407 important in re-circulating excess nutrients from the high-latitude oceans towards the low
408 latitude-regions of the Pacific Ocean. We suggest that the observed glacial changes in $\delta^{13}C$-
409 signatures of tropical intermediate waters in the ETNP are linked to additional contribution of
410 northern-sourced intermediate waters that further confirm considerations of a southward
411 expansion of GNPIW to explain the $\delta^{13}C$ signatures found in the mid-depth tropical Pacific
412 during MIS 2 [*Herguera et al.*, 2010].
413
414 4.2. Evidence for increased GNPIW influence on the Eastern Equatorial Pacific since MIS 2?
415 To assess whether GNPIW expanded further south to the equatorial upwelling system, we
416 compare the variability in $\delta^{13}C$ of GNPIW and AAIW with our new sub-thermocline $\delta^{13}C$ proxy
417 record of the deep-dwelling planktonic foraminifera *G. hexagonus* from ODP Site 1240. Glacial
418 variations in $\delta^{13}C$ of sub-thermocline water masses are interpreted as both changes in incoming
419 nutrients and export productivity in the surface ocean of the EEP. During MIS 3 (~ 60 – 30 ka)
420 the *G. hexagonus* $\delta^{13}C$ proxy record indicates the presence of relatively ^{13}C-enriched (nutrient-
421 depleted) water masses with low variability in $\delta^{13}C$ of sub-thermocline waters of the EEP (Fig.
422 6a). At the same time, GNPIW shows distinctly lower (more-nutrient-rich) $\delta^{13}C$ values with
423 higher temporal variability than EEP sub-surface waters. However, apparent similarities are
424 observed since ~ 29 ka at the beginning of MIS 2, where absolute $\delta^{13}C$ values as well as the
425 long-term trend indicate more nutrient-enriched sub-thermocline water masses recorded in $\delta^{13}C$

426 of *G. hexagonus* at ODP Site 1240, which closely follows the temporal evolution of the $\delta^{13}C$
427 signature advected towards the tropical Pacific via GNPIW (Fig. 6a).
428
429 Interestingly, another rapid switch to monotonically increasing $\delta^{13}C$ of *G. hexagonus* is visible
430 during the last deglaciation, which suggests a decoupling from northern-sourced intermediate
431 waters between ~ 17 – 15 ka. The transition from ^{13}C-depleted (more nutrient-enriched) to rather
432 ^{13}C-enriched (more nutrient-depleted) sub-surface water implies another significant change in
433 characteristics of source water masses along with changes in biological productivity in the EEP
434 during the last deglaciation (Fig. 6a and b). Simultaneously, intermediate waters in the North
435 Pacific became further ^{13}C-depleted and seems to be decoupled from sub-thermocline waters in
436 the EEP. This is in line with a study on surface ocean productivity at ODP Site 1240, which
437 showed that southern-sourced intermediate waters played a more dominant role for the nutrient
438 redistribution in the EEP since the early deglaciation [e.g. *Calvo et al.*, 2011]. Dissimilar trends
439 are also evident between northern-sourced intermediate water and mid-depth water masses in the
440 ETNP, probably due to a reduced lateral extent of GNPIW during the last deglaciation (Fig. 5a).
441 Since then, mid-depth waters in the ETNP seems to follow the temporal variability of southern-
442 sourced intermediate water that imply a larger influence of ^{13}C-enriched (more nutrient-depleted)
443 AAIW in the tropical Pacific. However, we note that large gradients between $\delta^{13}C$ of sub-
444 thermocline waters in the EEP and AAIW are also present during the last deglaciation and
445 Holocene. Still, available benthic $\delta^{13}C$ records from the mid-depth to deep North Pacific do not
446 cover the whole Holocene and impede further interpretation of $\delta^{13}C$ variability in the ETNP
447 during this time.
448

449 Past changes in sub-thermocline water mass signatures in the EEP have been usually linked to
450 differences in advection and/or source-water mass characteristics of Southern Ocean water
451 masses to the tropical Pacific. Rapid changes in meridional transport of southern-sourced
452 intermediate water towards the tropical regions have been proposed from εNd records over the
453 last 30 kyr [*Pena et al.*, 2013]. A recent study investigating Southern Ocean and EEP shallow-
454 and deep-water ventilation ages suggest that relatively old water masses (PDW/UCDW)
455 upwelled to EEP thermocline waters and proposed a dominant deep southern-source during late
456 MIS 2 [*de la Fuente et al.*, 2015]. A study reconstructing radiocarbon activity of mid-depth
457 waters from sediment cores off Baja California also pointed to the presence of slightly older
458 intermediate waters in the eastern North Pacific during the latter part of the glacial period
459 [*Marchitto et al.*, 2007], which might also explain glacial age anomalies in the surface ocean of
460 the EEP. Thus, we explain changes in $\delta^{13}C$ of sub-thermocline water masses of the EEP between
461 MIS 3 and MIS 2 by changes in source water masses characteristics probably due to variable
462 ocean interior transport pathways reaching the equatorial Pacific under glacial conditions. Based
463 on the apparent similarities between $\delta^{13}C$-signatures of northern-sourced intermediate waters,
464 mid-depth waters in the Panama basin of the ETNP and sub-thermocline waters in the EEP (Fig.
465 5a and 6a), we argue for additional intrusion of GNPIW into sub-thermocline water masses of
466 the EEP during MIS 2.
467
468 4.3. “North Pacific Nutrient Leakage”
469 We provide the first evidence that relatively ^{13}C-depleted (nutrient-enriched) GNPIW influenced
470 glacial EEP sub-thermocline waters during MIS 2 and discuss further potential implications on
471 marine productivity of the equatorial Pacific regions at that time (Fig. 6a - c). Nitrogen and

472 silicon isotopes are often used as diagnostic tools for reconstructing past nutrient cycling. With
473 higher nutrient consumption, both substrate (dissolved nutrients) and products generated from it
474 become progressively enriched in heavier isotopes [*Robinson et al.*, 2014]. Indeed, several
475 studies of sediment cores in the EEP found evidence for changes in marine productivity and
476 nutrient utilization during MIS 2 [*Kienast et al.*, 2007; *Pichevin et al.*, 2009; *Robinson et al.*,
477 2009; *Dubois et al.*, 2011] (Fig. 6b). Overall similarities between these records demonstrate that
478 they are not primarily influenced by local processes at the deposition site, but rather reflect a
479 robust signal of regional changes in nutrient delivery and biological productivity in the EEP
480 [*Dubois et al.*, 2011]. *Pichevin et al.* [2009] suggested that the glacial biological carbon pump in
481 the EEP was more efficient due to a relaxation of nutrient limitation and speculated about its
482 contribution to lower atmospheric CO_2 conditions during MIS 2.
483
484 Glacial relaxation of nutrient limitation and concurrent maxima in biological productivity in the
485 EEP have been usually related to the redistribution of excess nutrients (mainly silicic acid) from
486 the Southern Ocean via “ocean tunnelling” as proposed by the Silicic Acid Leakage Hypothesis
487 [*Matsumoto et al.*, 2002b]. At the same time, changes in the contribution of northern-sourced
488 intermediate waters are often neglected e.g. by assuming that the relative contribution from
489 northern- and southern-sourced water did not change significantly in the past [e.g. *Dubois et al.*,
490 2011; *Pena et al.*, 2013]. However, studies using diatom-bound silicon and nitrogen isotopes as
491 proxies for nutrient utilization suggested enhanced glacial drawdown of silicic acid and nitrate
492 along with higher glacial opal fluxes in the Pacific Subantarctic Zone of the Southern Ocean
493 during MIS 2 [*Bradtmiller et al.*, 2009; *Robinson et al.*, 2005, 2014]. These results show that, in
494 contrast to the EEP, silicic acid and nitrate have been utilized more efficiently and became rather

495 "trapped" north of the Antarctic Polar Front in the glacial deep Southern Ocean (Fig. 6b and c).
496 However, it has been also shown that average glacial opal fluxes were less than during the
497 Holocene south of the Antarctic Polar Front [*Bradtmiller et al.*, 2009]. Whether the glacial
498 Southern Ocean provides sufficient nutrients via "ocean tunnelling" to enhance marine
499 productivity at the EEP as predicted by the Silicic Acid Leakage Hypothesis is still controversial
500 [*Hendry and Brzezinski*, 2014*; Robinson et al.*, 2014].
501
502 Interestingly, times of enhanced organic carbon flux rates and low nutrient utilization (silicic
503 acid and nitrate) in the EEP are visible since the beginning of MIS 2 and generally coincided
504 with the proposed changes in additional contributions of relatively nutrient-rich GNPIW to
505 equatorial Pacific sub-thermocline water masses (Fig. 6b and c). Invoking an additional export of
506 unutilized (preformed) nutrients from the high-latitude North Pacific via nutrient-enriched
507 GNPIW (here named as "North Pacific Nutrient Leakage") thus might be another, yet
508 unconsidered, process to explain relieved nutrient limitation and a stimulated biological pump in
509 the EEP during MIS 2. Unfortunately, less is known about glacial changes in utilization of major
510 nutrients, such as silicon or iron in the source region of GNPIW. Some studies propose low
511 biological productivity and nutrient utilization (nitrate) in the Bering Sea due to a decrease in
512 productivity, or an increase in nitrate availability through changes in vertical mixing under
513 glacial conditions [*Riethdorf et al.*, 2013; *Schlung et al.*, 2013]. Other studies point to near-
514 complete nutrient utilization (nitrate) in the Bering Sea and western subarctic Pacific during
515 glacial times [*Brunelle et al.*, 2007, 2010]. A recent study emphasizes the role of strong physical
516 stratification of the glacial subarctic Pacific surface waters, which prevented additional flux of
517 nitrate from underlying water, such that available surface nitrate was used to near completion

518 [*Knudson and Ravelo*, 2015b]. Our results propose that additional influence of nutrient-rich
519 North Pacific mid-depth waters to the tropical Pacific via GNPIW might hold new clues about
520 glacial productivity changes in the EEP, but need to be further evaluated in order to understand
521 the role of enhanced influence of GNPIW to the low-latitude Pacific under glacial conditions.
522
523 During the deglaciation, the resumption of intense overturning within the Southern Ocean led to
524 a higher injection of relatively nutrient-depleted southern-sourced water masses into the EqPIW.
525 As a consequence, decreasing nutrient concentrations and increasing nutrient consumption are
526 recorded in the EqPIW (Fig. 6). However, we can only speculate about the offset in timing
527 between the onset of EqPIW $\delta^{13}C$ changes (shown by *G. hexagonus*) and the increase in $\delta^{15}N$ in
528 ODP Site 1240. The switch in relative end-member contribution during the deglaciation possibly
529 causes variations in intermediate water suboxia and hence water column denitrification
530 [*Robinson et al.*, 2009]. This would affect the nitrogen isotopes only as *G. hexagonus* seems to
531 be more insensitive to varying oxygen concentrations [*Rippert et al.*, 2016]. Nonetheless, the
532 discrepancy in timing needs to be further investigated in combination with $\delta^{15}N$ studies from the
533 subarctic Pacific.
534

535 **5 Conclusions**

536 Here we report on new foraminiferal $\delta^{13}C$ records from the western subarctic Pacific (Bering
537 Sea) and EEP spanning the past 60 kyr. Combined evidence of $\delta^{13}C$ from core SO201-2-101KL
538 and εNd records of the Bering Sea points to a long-term increase in GNPIW formation since the
539 onset of MIS 3, which culminated early in MIS 2 (~ 29 ka). The comparison between benthic
540 foraminiferal $\delta^{13}C$ records of SO201-2-101KL and marine sediment core MD02-2529 from the

Panama Basin as well as εNd records of the Bering Sea and eastern North Pacific reveals remarkable similarities in the long-term evolution between GNPIW and EqPIW signatures in the tropical North Pacific during the glacial period. These results support the notion that northern-sourced intermediate water extended further south to the tropical Pacific region than today under glacial boundary conditions. Glacial changes in $\delta^{13}C$ of sub-thermocline water masses in the EEP were derived from deep-dwelling planktonic foraminiferal species *G. hexagonus* at ODP Site 1240 and indicate significant changes in sub-thermocline water mass characteristics during MIS 2. Notably, the proposed times of additional influence of GNPIW to the tropical Pacific coincides with changes in nutrient availability and biological productivity in the glacial EEP. Overall, our new findings indicate that past changes in North Pacific mid-depth circulation might have played a crucial role in glacial nutrient availability and biological productivity in the EEP, but needs to be further constrained by future studies investigating glacial changes in utilization of major nutrients, such as silicon or iron in the subarctic Pacific.

Acknowledgments and Data

The Helmholtz Climate Initiative REKLIM (Regional climate change) funded this study. NR, LLJ and RT received funding through research projects Manihiki II (03G0225B) and SiGePAX (03F0704A) by the Bundesministerium für Bildung und Forschung (BMBF). This research used samples provided by BMBF-project KALMAR, and the International Ocean Discovery Program (IODP). IODP was sponsored by the U.S. National Science Foundation (NSF) and participating countries under the management of Joint Oceanographic Institutions (JOI), Inc. We gratefully acknowledge the Master and crew of R/V SONNE cruises SO201-2 (KALMAR) and thank for

their professional support on board. We express our thanks to L. Schönborn and G. Meyer for conducting stable isotope measurements at the AWI stable isotope lab. The authors thank Isabel Cacho and Helen Bostock for helpful comments and suggestions. We also would like to thank the anonymous reviewer, who helped to improve the quality of this manuscript. Supplementary data are available at PANGAEA Data Publisher for Earth & Environmental Science (https://www.pangaea.de).

References

Andersen, K.K., N. Azuma, J.M. Barnola, M. Bigler, P. Biscaye, N. Caillon, J. Chappellaz, H.B. Clausen, D. Dahl-Jensen, H. Fischer, J. Fluckiger, D. Fritzsche, Y. Fujii, K. Goto-Azuma, K. Gronvold, N.S. Gundestrup, M. Hansson, C. Huber, C.S. Hvidberg, S.J. Johnsen, U. Jonsell, J. Jouzel, S. Kipfstuhl, A. Landais, M. Leuenberger, R. Lorrain, V. Masson-Delmotte, H. Miller, H. Motoyama, H. Narita, T. Popp, S.O. Rasmussen, D. Raynaud, R. Rothlisberger, U. Ruth, D. Samyn, J. Schwander, H. Shoji, M.L. Siggard-Andersen, J.P. Steffensen, T. Stocker, A.E. Sveinbjornsdottir, A. Svensson, M. Takata, J.L. Tison, T. Thorsteinsson, O. Watanabe, F. Wilhelms, J.W.C. White, and N.G.I.C. Project (2004), High-resolution record of Northern Hemisphere climate extending into the last interglacial period, Nature 431, 147-151.

Antonov, J.I., D. Seidov, T.P. Boyer, R.A. Locarnini, A.V. Mishonov, H.E. Garcia, O.K. Baranova, M.M. Zweng, and D.R. Johnson (2010), World Ocean Atlas 2009, Volume 2: Salinity. S. Levitus (Ed.), NOAA Atlas NESDIS 69, U.S. Government Printing Office, Washington D.C., 184 pp.

Basak, C., E.E. Martin, K. Horikawa, and T.M. Marchitto (2010), Southern Ocean source of superset of ^{14}C-depleted carbon in the North Pacific Ocean during the last deglaciation, Nature Geoscience 3(11), 770-773.

Bemis, B.E., H.J. Spero, J. Bijma, and D.W. Lea (1998), Reevaluation of the oxygen isotopic composition of planktonic foraminifera: Experimental results and revised paleotemperature equations. Paleoceanography 13, 150-160.

Bostock, H.C., B.N. Opdyke, and M.J.M. Williams (2010), Characterising the intermediate depth waters of the Pacific Ocean using δ^{13}C and other geochemical tracers. Deep-Sea Research Part I-Oceanographic Research Papers 57(7), 847-85.

Bradtmiller, L.I., R.F. Anderson, M.Q. Fleisher, and L.H. Burckle (2009), Comparing glacial

601 and Holocene opal fluxes in the Pacific sector of the Southern Ocean. Paleoceanography
602 24, PA2214, doi:10.1029/2008PA001693.
603
604 Brunelle, B.G., D.M. Sigman, M.S. Cook, L.D. Keigwin, G.H. Haug, B. Plessen, G. Schettler,
605 and S.L. Jaccard (2007), Evidence from diatom-bound nitrogen isotopes for subarctic
606 Pacific stratification during the last ice age and a link to North Pacific denitrification
607 changes. Paleoceanography 22, PA1215, doi:10.1029/2005PA001205.
608
609 Brunelle, B.G., D.M. Sigman, S.L. Jaccard, L.D. Keigwin, B. Plessen, G. Schettler, M.S. Cook,
610 and G.H. Haug (2010), Glacial/interglacial changes in nutrient supply and stratification in
611 the western subarctic North Pacific since the penultimate glacial maximum. Quaternary
612 Science Reviews 29, 2579-2590.
613
614 Calvo, E., C. Pelejero, L.D. Pena, I. Cacho, and G.A. Logan (2011), Eastern Equatorial Pacific
615 productivity and related-CO_2 changes since the last glacial period. Proceedings of the
616 National Academy of Sciences of the United States of America 108, 5537-5541.
617
618 Carriquiry, J.e.D., A. Sanchez, and G. Leduc (2015), Southern Ocean influence on the Eastern
619 Tropical North Pacific's intermediate depth circulation during the last glacial maximum.
620 Paleoceanography 30, 1132–1151.
621
622 Curry, W.B., J.C. Duplessy, L.D. Labeyrie, and N.J. Shackleton (1988), Changes in the
623 distribution of $\delta^{13}C$ of deep water Sigma CO_2 between the last glaciation and the
624 Holocene. Paleoceanography 3(3), 317-341.
625
626 Curry, W.B., and D.W. Oppo (2005), Glacial water mass geometry and the distribution of $\delta^{13}C$
627 of Sigma CO_2 in the western Atlantic Ocean. Paleoceanography 20(1), PA1017,
628 doi:10.1029/2004PA001021
629
630 de la Fuente, M., L. Skinner, E. Calvo, C. Pelejero, and I. Cacho (2015), Increased reservoir ages
631 and poorly ventilated deep waters inferred in the glacial Eastern Equatorial Pacific.
632 Nature Communications 6, 7420, doi:10.1038/ncomms8420.
633
634 Dubois, N., M. Kienast, S. Kienast, C. Normandeau, S.E. Calvert, T.D. Herbert, and A. Mix
635 (2011), Millennial-scale variations in hydrography and biogeochemistry in the Eastern
636 Equatorial Pacific over the last 100 kyr. Quaternary Science Reviews 30, 210-223.
637
638 Dugdale, R.C., A.G. Wischmeyer, F.P. Wilkerson, R.T. Barber, F. Chai, M.S. Jiang, and T.H.
639 Peng (2002), Meridional asymmetry of source nutrients to the equatorial Pacific
640 upwelling ecosystem and its potential impact on ocean-atmosphere CO(2) flux; a data
641 and modeling approach. Deep-Sea Research Part II-Topical Studies in Oceanography 49,
642 2513-2531.
643
644 Duplessy, J.C., N.J. Shackleton, R.K. Matthews, W. Prell, W.F. Ruddiman, M. Caralp, and C.H.

Hendy (1984), C-13 Record of Benthic Foraminifera in the Last Interglacial Ocean - Implications for the Carbon-Cycle and the Global Deep-Water Circulation. Quaternary Research 21, 225-243.

Duplessy, J.C., N.J. Shackleton, R.G. Fairbanks, L. Labeyrie, D. Oppo, and N. Kallel (1988), Deepwater source variations during the last climatic cycle and their impact on the global deepwater circulation. Paleoceanography 3, 343-360.

Epstein, S., R.H. Buchsbaum, A. Lowenstam, and H.C. Urey (1953), Revised carbonate-water isotopic temperature scale. Geological Society of America Bulletin 64, 1315-1325.

Galbraith, E.D., S.L. Jaccard, T.F. Pedersen, D.M. Sigman, G.H. Haug, M. Cook, J.R. Southon, and R. Francois (2007), Carbon dioxide release from the North Pacific abyss during the last deglaciation. Nature 449, 890-894.

Garcia, H.E., R.A. Locarnini, T.P. Boyer, J.I. Antonov, M.M. Zweng, O.K. Baranova, and D.R. Johnson (2010), World Ocean Atlas 2009, Volume 4: Nutrients (phosphate, nitrate, silicate). S. Levitus (Ed.), NOAA Atlas NESDIS, 71, U.S. Government Printing Office, Washington D.C., 398 pp.

Haug, G.H., D.M. Sigman, R. Tiedemann, T.F. Pedersen, and M. Sarnthein (1999), Onset of permanent stratification in the subarctic Pacific Ocean. Nature 401(6755), 779-782.

Hendry, K.R., and M.A. Brzezinski (2014), Using silicon isotopes to understand the role of the Southern Ocean in modern and ancient biogeochemistry and climate. Quaternary Science Reviews 89, 13-26.

Herguera, J.C., E. Jansen, and W.H. Berger (1992), Evidence for a Bathyal Front at 2000-M Depth in the Glacial Pacific, Based on a Depth Transect on Ontong Java Plateau. Paleoceanography 7, 273-288.

Herguera, J.C., T. Herbert, M. Kashgarian, and C. Charles (2010), Intermediate and deep water mass distribution in the Pacific during the Last Glacial Maximum inferred from oxygen and carbon stable isotopes. Quaternary Science Reviews 29, 1228-1245.

Hu, R., A.M. Piotrowski, H.C. Bostock, S. Crowhurst, and V. Rennie (2016), Variability of neodymium isotopes associated with planktonic foraminifera in the Pacific Ocean during the Holocene and Last Glacial Maximum. Earth and Planetary Science Letters 447, 130-138.

Honda, M.C., K. Imai, Y. Nojiri, F. Hoshi, T. Sugawara, and M. Kusakabe (2002), The biological pump in the northwestern North Pacific based on fluxes and major components of particulate matter obtained by sediment-trap experiments (1997-2000). Deep-Sea Research Part II-Topical Studies in Oceanography 49, 5595-5625.

Horikawa, K., Y. Asahara, K. Yamamoto, and Y. Okazaki (2010), Intermediate water formation

691 in the Bering Sea during glacial periods: Evidence from neodymium isotope ratios.
692 Geology 38, 435-438.
693
694 Keigwin, L.D. (1998), Glacial-age hydrography of the far northwest Pacific Ocean.
695 Paleoceanography 13, 323-339.
696
697 Kennett, J.P., and B.L. Ingram (1995), A 20,000 Year Record of Ocean Circulation and Climate-
698 Change from the Santa-Barbara Basin. Nature 377, 510-514.
699
700 Key, R.M., A. Kozyr, C.L. Sabine, K. Lee, R. Wanninkhof, J.L. Bullister, R.A. Feely, F.J.
701 Millero, C. Mordy, and T.H. Peng (2004), A global ocean carbon climatology: Results
702 from Global Data Analysis Project (GLODAP). Global Biogeochemical Cycles 18,
703 GB4031, doi:10.1029/2004GB002247.
704
705 Kienast, S.S., M. Kienast, A.C. Mix, S.E. Calvert, and R. Francois (2007), Thorium-230
706 normalized particle flux and sediment focusing in the Panama Basin region during the
707 last 30,000 years. Paleoceanography 22(2), PA2213, doi:10.1029/2006PA001357.
708
709 Kim, S.T., and J.R. O'Neil (1997), Equilibrium and nonequilibrium oxygen isotope effects in
710 synthetic carbonates. Geochimica Et Cosmochimica Acta 61, 3461-3475.
711
712 Knudson, K.P., and A.C. Ravelo (2015a), North Pacific Intermediate Water circulation enhanced
713 by the closure of the Bering Strait. Paleoceanography 30, 1-18.
714
715 Knudson, K.P., and A.C.Ravelo (2015b), Enhanced subarctic Pacific stratification and nutrient
716 utilization during glacials over the last 1.2Myr. Geophysical Research Letters 42, 9870-
717 9879.
718
719 Kroopnick, P.M. (1985), The Distribution of ^{13}C of $\sum CO_2$ in the World Oceans. Deep-
720 Sea Research Part a-Oceanographic Research Papers 32, 57-84.
721
722 Leduc, G., L. Vidal, K. Tachikawa, F. Rostek, C. Sonzogni, L. Beaufort, and E. Bard (2007),
723 Moisture transport across Central America as a positive feedback on abrupt climatic
724 changes. Nature 445, 908-911.
725
726 Leduc, G., L. Vidal, K. Tachikawa, and E. Bard (2010), Changes in Eastern Pacific ocean
727 ventilation at intermediate depth over the last 150 kyr BP. Earth and Planetary Science
728 Letters 298, 217-228.
729
730 Locarnini, R.A., A.V. Mishonov, J.I. Antonov, T.P. Boyer, H.E. Garcia, O.K. Baranova, M.M.
731 Zweng, and D.R. Johnson (2010), World Ocean Atlas 2009, Volume 1: Temperature. S.
732 Levitus (Ed.), NOAA Atlas NESDIS, 68, U.S. Government Printing Office, Washington
733 D.C., 184 pp.
734
735 Lund, D.C., and A.C. Mix (1998), Millennial-scale deep water oscillations: Reflections of the
736 North Atlantic in the deep Pacific from 10 to 60 ka. Paleoceanography 13(1), 10-19.
737

738 Lynch-Stieglitz, J., R.G. Fairbanks, and C.D. Charles (1994), Glacial-interglacial history of
739 Antarctic Intermediate Water: Relative strengths of Antarctic versus Indian Ocean
740 sources. Paleoceanography 9(1), 7-29. doi:10.1029/93PA02446.
741
742 Mackensen, A., S. Schumacher, J. Radke, and D.N. Schmidt (2000), Microhabitat preferences
743 and stable carbon isotopes of endobenthic foraminifera: clue to quantitative
744 reconstruction of oceanic new production? Marine Micropaleontology 40, 233-258.
745
746 Marchitto, T.M., S.J. Lehman, J.D. Ortiz, J. Fluckiger, and A. van Geen (2007), Marine
747 radiocarbon evidence for the mechanism of deglacial atmospheric CO_2 rise. Science 316,
748 1456-1459.
749
750 Matsumoto, K., T. Oba, J. Lynch-Stieglitz, and H. Yamamoto (2002a), Interior hydrography and
751 circulation of the glacial Pacific Ocean. Quaternary Science Reviews 21, 1693-1704.
752
753 Matsumoto, K., J.L. Sarmiento, and M.A. Brzezinski (2002b), Silicic acid leakage from the
754 Southern Ocean: A possible explanation for glacial atmospheric pCO_2. Global
755 Biogeochemical Cycles 16, 1031, doi:10.1029/2001GB001442.
756
757 Max, L., J.R. Riethdorf, R. Tiedemann, M. Smirnova, L. Lembke-Jene, K. Fahl, D. Nürnberg, A.
758 Matul, and G. Mollenhauer (2012), Sea surface temperature variability and sea-ice extent
759 in the subarctic northwest Pacific during the past 15,000 years. Paleoceanography 27,
760 PA3213, doi:10.1029/2012PA002292.
761
762 Max, L., L. Lembke-Jene, J.R. Riethdorf, R. Tiedemann, D. Nürnberg, H. Kühn, and A.
763 Mackensen (2014), Pulses of enhanced North Pacific Intermediate Water ventilation from
764 the Okhotsk Sea and Bering Sea during the last deglaciation. Climate of the Past 10, 591-
765 605.
766
767 Méheust, M., R. Stein, K. Fahl, L. Max, and J.R. Riethdorf (2016), High- resolution IP_{25}-based
768 reconstruction of sea-ice variability in the western North Pacific and Bering Sea during
769 the past 18,000 years. Geo-Marine Letters 36(2), 1-11.
770
771 Mix, A.C., N.G. Pisias, R. Zahn, W. Rugh, C. Lopez, and K. Nelson (1991), Carbon 13 in
772 Pacific deep and intermediate waters, 0-370 ka: Implications for ocean circulation and
773 Pleistocene CO_2. Paleoceanography 6(2), 205-226.
774
775 Mook, W.G., J.C. Bommerso, and W.H. Staverma (1974), Carbon Isotope Fractionation between
776 Dissolved Bicarbonate and Gaseous Carbon-Dioxide. Earth Planetary Science Letters 22,
777 169-176.
778
779 Muratli, J.M., Z. Chase, A.C. Mix, and J. McManus (2010), Increased glacial-age ventilation of
780 the Chilean margin by Antarctic Intermediate Water. Nature Geoscience 3(1), 23-26.
781
782 Noble, T.L., A.M. Piotrowski, and I.N. McCave (2013), Neodymium isotopic composition of

783 intermediate and deep waters in the glacial southwest Pacific. Earth and Planetary
784 Science Letters 384, 27-36.
785
786 Okazaki, Y., T. Sagawa, H. Asahi, K. Horikawa, and J. Onodera (2012), Ventilation changes in
787 the western North Pacific since the last glacial period. Climate of the Past 8, 17-24.
788
789 Ortiz, J.D., A.C. Mix, W. Rugh, J.M. Watkins, and R.W. Collier (1996), Deep-dwelling
790 planktonic foraminifera of the northeastern Pacific Ocean reveal environmental control of
791 oxygen and carbon isotopic disequilibria. Geochimica Et Cosmochimica Acta 60, 4509-
792 4523.
793
794 Pahnke, K., and R. Zahn (2005), Southern hemisphere water mass conversion linked with North
795 Atlantic climate variability. Science 307, 1741-1746.
796
797 Pena, L.D., I. Cacho, P. Ferretti, and M.A. Hall (2008), El Nino-Southern Oscillation-like
798 variability during glacial terminations and interlatitudinal teleconnections.
799 Paleoceanography 23, PA3101, doi:10.1029/2008PA001620.
800
801 Pena, L.D., S.L. Goldstein, S.R. Hemming, K.M. Jones, E. Calvo, C. Pelejero, and I. Cacho
802 (2013), Rapid changes in meridional advection of Southern Ocean intermediate waters to
803 the tropical Pacific during the last 30 kyr. Earth and Planetary Science Letters 368, 20-32.
804
805 Petit, J.R., J. Jouzel, D. Raynaud, N.I. Barkov, J.M. Barnola, I. Basile, M. Bender, J. Chappellaz,
806 M. Davis, G. Delaygue, M. Delmotte, V.M. Kotlyakov, M. Legrand, V.Y. Lipenkov, C.
807 Lorius, L. Pepin, C. Ritz, E. Saltzman, and M. Stievenard (1999), Climate and
808 atmospheric history of the past 420,000 years from the Vostok ice core, Antarctica.
809 Nature 399, 429-436.
810
811 Pichevin, L.E., B.C. Reynolds, R.S. Ganeshram, I. Cacho, L. Pena, K. Keefe, and R.M. Ellam
812 (2009), Enhanced carbon pump inferred from relaxation of nutrient limitation in the
813 glacial ocean. Nature 459, 1114-1118.
814
815 Rafter, P. A., and D. M. Sigman (2016), Spatial distribution and temporal variation of nitrate
816 nitrogen and oxygen isotopes in the upper equatorial Pacific Ocean, Limnol Oceanogr,
817 61(1), 14-31.
818
819 Rella, S.F., R. Tada, K. Nagashima, M. Ikehara, T. Itaki, K. Ohkushi, T. Sakamoto, N. Harada,
820 and M. Uchida (2012), Abrupt changes of intermediate water properties on the
821 northeastern slope of the Bering Sea during the last glacial and deglacial period.
822 Paleoceanography 27, PA3203, doi:10.1029/2011PA002205.
823
824 Riethdorf, J.R., D. Nürnberg, L. Max, R. Tiedemann, S.A. Gorbarenko, and M.I. Malakhov
825 (2013), Millennial-scale variability of marine productivity and terrigenous matter supply
826 in the western Bering Sea over the past 180 kyr. Climate of the Past 9, 1345-1373.
827

828 Rippert, N., D. Nürnberg, J. Raddatz, E. Maier, E. Hathorne, J. Bijma, and R. Tiedemann (2016),
829 Constraining foraminiferal calcification depths in the western Pacific warm pool. Marine
830 Micropaleontology, 128, 14-27.
831
832 Robinson, R.S., D.M. Sigman, P.J. DiFiore, M.M. Rohde, T.A. Mashiotta, and D.W. Lea (2005),
833 Diatom-bound N-15/N-14: New support for enhanced nutrient consumption in the ice age
834 subantarctic. Paleoceanography 20, PA3003, doi:10.1029/2004PA001114.
835
836 Robinson, R.S., P. Martinez, L.D. Pena, and I. Cacho (2009), Nitrogen isotopic evidence for
837 deglacial changes in nutrient supply in the eastern equatorial Pacific. Paleoceanography
838 24, PA4213, doi:10.1029/2008PA001702.
839
840 Robinson, R.S., M.A. Brzezinski, C.P. Beucher, M.G.S. Horn, and P. Bedsole (2014), The
841 changing roles of iron and vertical mixing in regulating nitrogen and silicon cycling in
842 the Southern Ocean over the last glacial cycle. Paleoceanography 29, 1179-1195.
843
844 Ronge, T.A., S. Steph, R. Tiedemann, M. Prange, U. Merkel, D. Nürnberg, and G. Kuhn (2015),
845 Pushing the boundaries: Glacial/interglacial variability of intermediate and deep waters in
846 the southwest Pacific over the last 350,000 years. Paleoceanography 30, 23-38.
847
848 Sarmiento, J.L., N. Gruber, M.A. Brzezinski, and J.P. Dunne (2004), High-latitude controls of
849 thermocline nutrients and low latitude biological productivity. Nature 427, 56-60.
850
851 Schlitzer, R. (2015), Data Analysis and Visualization with Ocean Data View. CMOS Bulletin
852 SCMO 43 (1), 9-13.
853
854 Schlung, S.A., A.C. Ravelo, I.W. Aiello, D.H. Andreasen, M.S. Cook, M. Drake, K.A. Dyez,
855 T.P. Guilderson, J.P. LaRiviere, Z. Stroynowski, and K. Takahashi (2013), Millennial-
856 scale climate change and intermediate water circulation in the Bering Sea from 90 ka: A
857 high-resolution record from IODP Site U1340. Paleoceanography 28, 54–67.
858
859 Schweizer, M., J. Pawlowski, T. Kouwenhoven, and B. van der Zwaan (2009), Molecular
860 Phylogeny of Common Cibicidids and Related Rotaliida (Foraminifera) Based on Small
861 Subunit eDNA Sequences. Journal of Foraminiferal Research 39, 300-315.
862
863 Shackleton, N.J. (1974), Attainment of isotopic equilibrium between ocean water and the benthic
864 foraminifera genus Uvigerina: isotopic changes in the ocean during the last glacial.
865 Centre National de la Recherche Scientifique Colloqium International 219, 203-209.
866
867 Shcherbina, A.Y., L.D. Talley, and D.L. Rudnick (2003), Direct observations of North Pacific
868 ventilation: Brine rejection in the Okhotsk Sea. Science 302(5652), 1952-1955.
869
870 Spero, H.J., and D.W. Lea (2002), The Cause of Carbon Isotope Minimum Events on Glacial
871 Terminations, Science, 296(5567), 522-525. doi:10.1126/science.1069401.
872
873 Stott, L.D., M. Neumann, and D. Hammond (2000), Intermediate water ventilation on the

874 northeastern Pacific margin during the late Pleistocene inferred from benthic
875 foraminiferal $\delta^{13}C$. Paleoceanography 15, 161-169.
876
877 Stott, L., J. Southon, A. Timmermann, and A. Koutavas (2009), Radiocarbon age anomaly at
878 intermediate water depth in the Pacific Ocean during the last deglaciation.
879 Paleoceanography 24, PA2223, doi:10.1029/2008PA001690.
880
881 Svensson, A., K.K. Andersen, M. Bigler, H.B. Clausen, D. Dahl-Jensen, S.M. Davies, S.J.
882 Johnsen, R. Muscheler, F. Parrenin, S.O. Rasmussen, R. Roethlisberger, I. Seierstad, J.P.
883 Steffensen, and B.M. Vinther (2008), A 60 000 year Greenland stratigraphic ice core
884 chronology. Climate of the Past 4, 47-57.
885
886 Takahashi, T., S.C. Sutherland, C. Sweeney, A. Poisson, N. Metzl, B. Tilbrook, N. Bates, R.
887 Wanninkhof, R.A. Feely, C. Sabine, J. Olafsson, and Y. Nojiri (2002), Global sea-air
888 CO_2 flux based on climatological surface ocean pCO_2, and seasonal biological and
889 temperature effects. Deep-Sea Research Part II-Topical Studies in Oceanography 49,
890 1601-1622.
891
892 Talley, L. D. (1993), Distribution and Formation of North Pacific Intermediate Water, Journal of
893 Physical Oceanography 23(3), 517-537.
894
895 Tanaka, S., and K. Takahashi (2005), Late Quaternary paleoceanographic changes in the Bering
896 Sea and the western subarctic Pacific based on radiolarian assemblages. Deep-Sea
897 Research Part II-Topical Studies in Oceanography 52(16-18), 2131-2149.
898
899 Wejnert, K.E., R.C. Thunell, and Y. Astor (2013), Comparison of species-specific oxygen
900 isotope paleotemperature equations: Sensitivity analysis using planktonic foraminifera
901 from the Cariaco Basin, Venezuela. Marine Micropaleontology 101, 76-88.
902

Figures

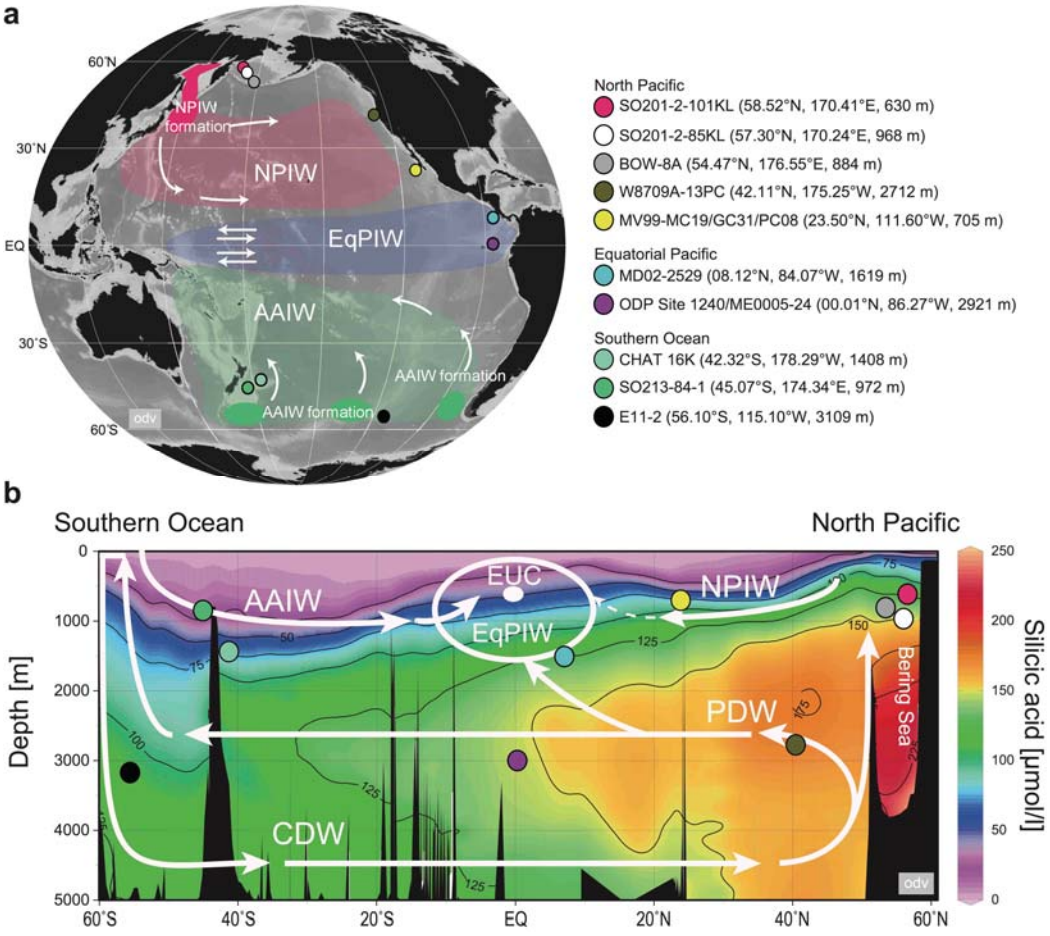

Figure 1 a: Bathymetric chart of the Pacific Ocean with locations of proxy records in the North Pacific (SO201-2-101KL, *this study*; SO201-2-85KL, *Max et al.*, 2012; BOW-8A, *Horikawa et al.*, 2010; W8709A-13PC, *Lund and Mix*, 1998; MV99-MC19/GC31/PC08, *Basak et al.*, 2010), the Equatorial Pacific (MD02-2529, *Leduc et al.*, 2010; ODP Site 1240, *Pichevin et al.*, 2009; *this study*; ME0005-24, *Kienast et al.*, 2007), and the Southern Ocean (CHAT 16K, *Noble et al.*, 2013; SO213-84-1, *Ronge et al.*, 2015; E11-2, *Robinson et al.*, 2014) considered in this study. White arrows denote major circulation pattern of intermediate water masses in the North Pacific and Southern Ocean: Magenta and green spots indicate formation regions of AAIW and NPIW, shaded magenta and green areas mark modern lateral extent of intermediate waters in the Pacific Ocean. b: Meridional section of present-day silicic acid concentrations from the North Pacific to the Southern Ocean [*Garcia et al.*, 2010] and major modern mid-depth to deep-water masses (white arrows): AAIW = Antarctic Intermediate Water; CDW = Circumpolar Deep Water; EUC = Equatorial Undercurrent; EqPIW = Equatorial Pacific Intermediate Water; NPIW = North Pacific Intermediate water; PDW = Pacific Deep Water [modified after *Bostock et al.*, 2010]. This figure was generated with Ocean Data View [*Schlitzer*, 2015].

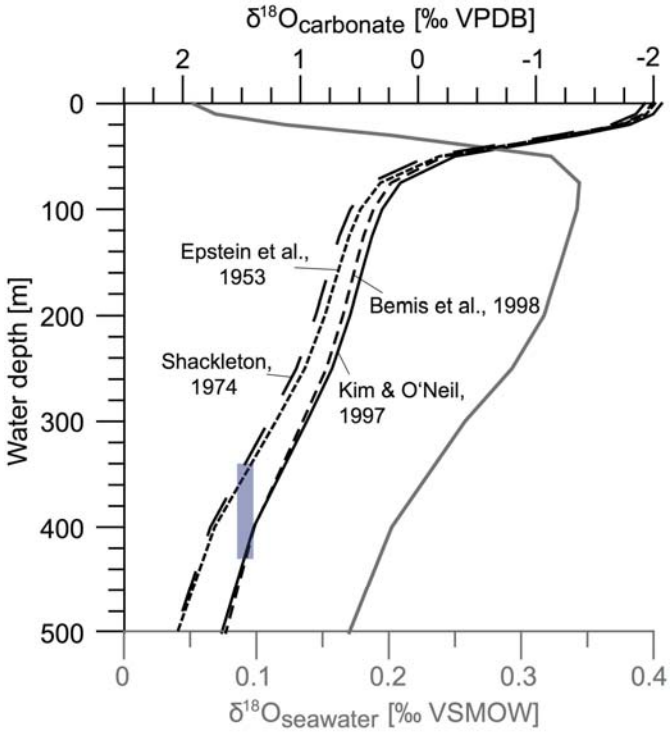

Figure 2 Apparent calcification depth (ACD) of planktonic foraminifera *G. hexagonus* in the Eastern Equatorial Pacific. ACD of *G. hexagonus* at ODP Site 1240 was inferred from best match between measured foraminiferal $\delta^{18}O_{calcite}$ values and corresponding calculated theoretically present $\delta^{18}O_{equilibrium}$ value, which were determined using various paleotemperature equations (black partly dashed lines), modern water temperatures [*Locarnini et al.*, 2010] and $\delta^{18}O_{seawater}$ (gray line). The blue bar indicates the ACD range of *G. hexagonus* considering all used equations.

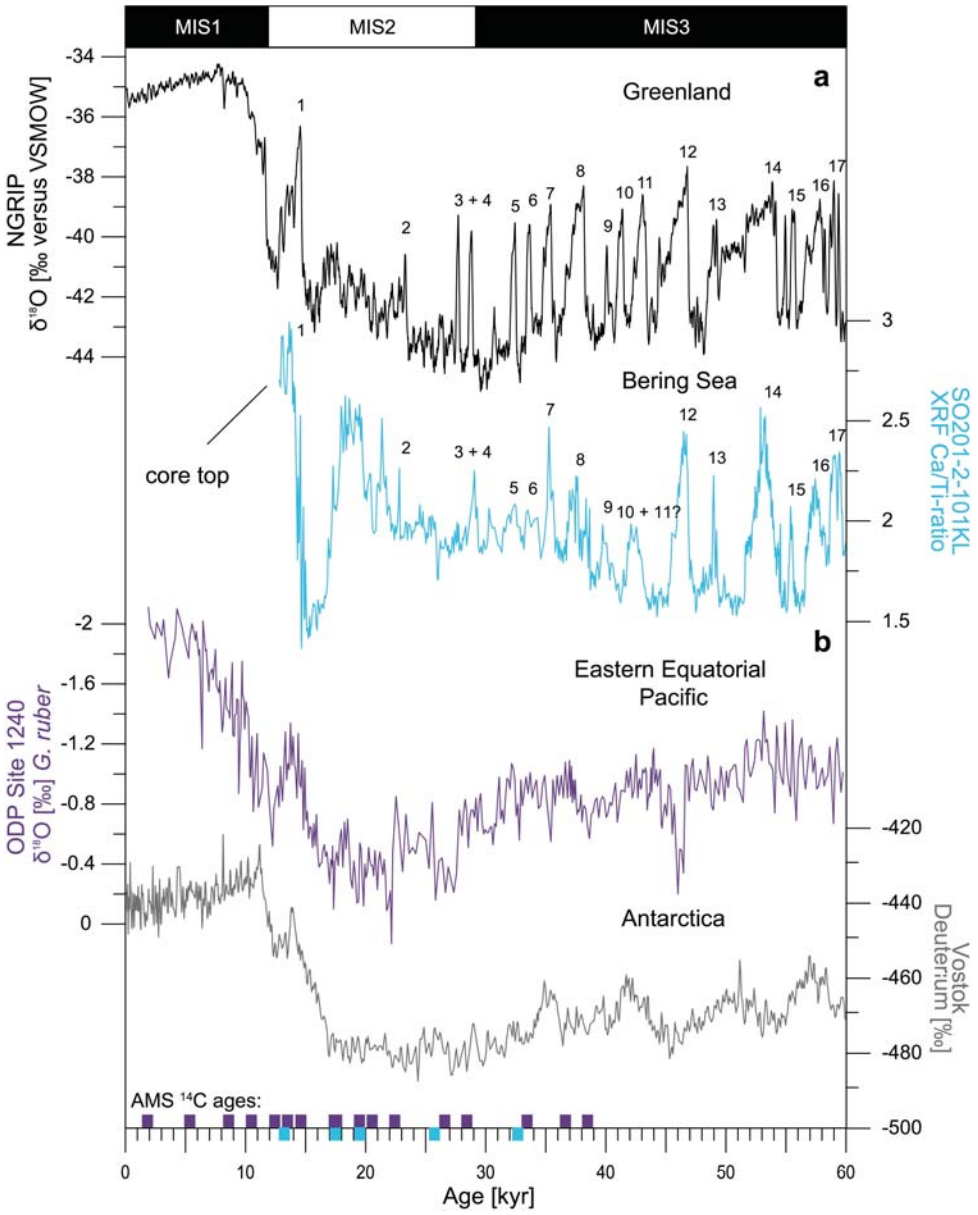

Figure 3 a: Comparison of high-resolution XRF core-logging data (Ca/Ti-ratio) from core SO201-2-101KL to NGRIP ice-core record. Numbers indicate Dansgaard-Oeschger Interstadials in NGRIP [*Andersen et al.*, 2004] and SO201-2-101KL (this study) during the past 60 kyr [*Riethdorf et al.*, 2013]. b: The stratigraphic framework of ODP Site 1240 based on 17 AMS ^{14}C ages and graphical tuning deeper parts of the cores to the Vostok ice core record [*Petit et al.*, 1999; *Pena et al.*, 2008]. Available AMS-^{14}C dating's derived from core SO201-2-101KL and ODP Site 1240 are given by blue and purple squares at the bottom.

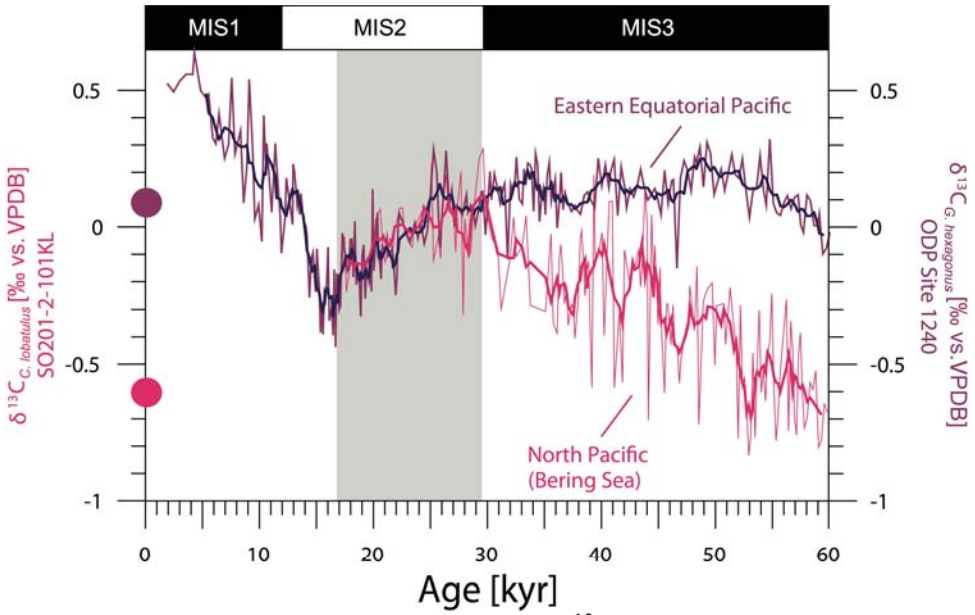

Figure 4 Detailed comparison of mid-depth benthic $\delta^{13}C$ record from sediment core SO201-2-101KL from the subarctic Pacific (Bering Sea) with $\delta^{13}C$ record of deep-dwelling (sub-thermocline) planktonic foraminifera *G .hexagonus* derived from ODP Site 1240 in the Eastern Equatorial Pacific during the past 60 kyr. Gray shaded area marks times of convergence between the given $\delta^{13}C$ records during MIS 2. Coloured circles indicate $\delta^{13}C_{DIC}$ composition of water masses bathing the respective core sites under modern conditions [*Key et al.*, 2004].

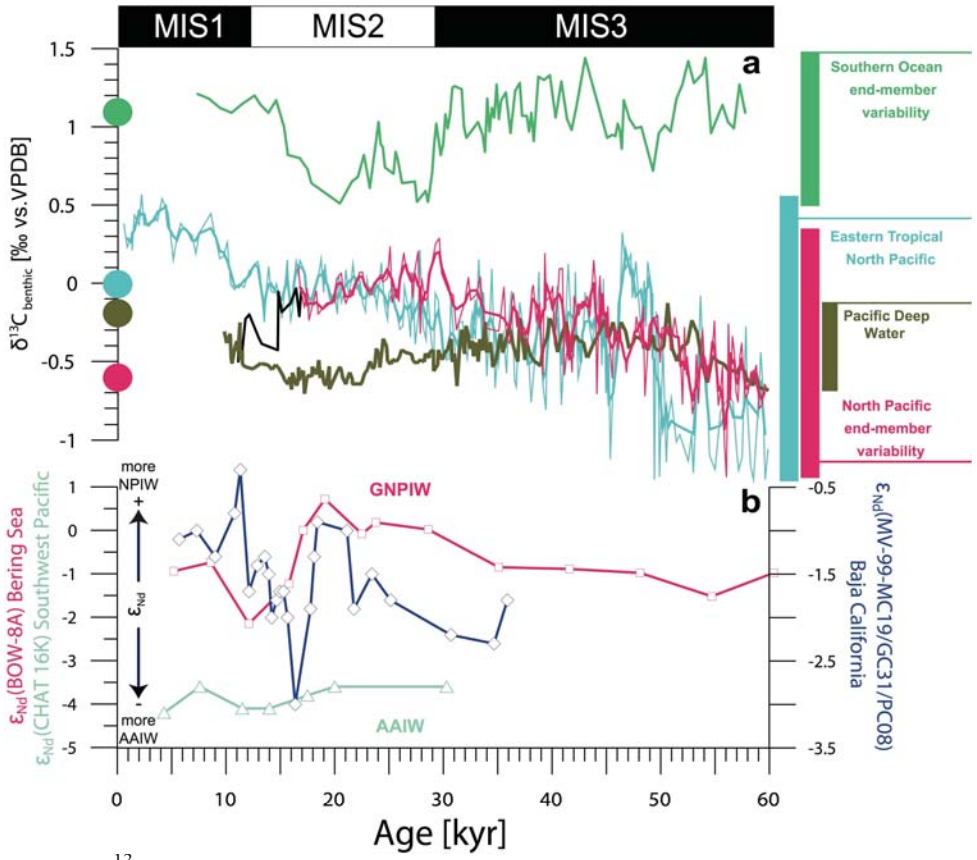

Figure 5 Benthic $\delta^{13}C$ records and εNd signatures from intermediate waters of the North Pacific (GNPIW), off Baja California, the Eastern Tropical North Pacific (EqPIW) and the Southern Ocean (AAIW) compared to benthic $\delta^{13}C$ deep-water (PDW) variability for the last 60 kyr. a: Benthic $\delta^{13}C$ record from Southern Ocean core SO213-84-1 (AAIW, in green) [*Ronge et al.*, 2015], benthic $\delta^{13}C$ record from MD02-2529 located in the Eastern Tropical North Pacific (in light blue) [*Leduc et al.*, 2010], benthic intermediate-water $\delta^{13}C$ record from Bering Sea core SO201-2-101KL (in magenta; this study) and SO201-2-85KL (in black) [*Max et al.*, 2014], deep-water benthic $\delta^{13}C$ record from core W8709A-13PC (in brown) [*Lund and Mix*, 1998) b: End-member intermediate-water mass εNd records from southern Bering Sea core BOW-8A (GNPIW, in magenta) [*Horikawa et al.*, 2010] and Southwest Pacific core CHAT 16K (AAIW, in light green) [*Noble et al.*, 2013] together with εNd signatures derived from sediment cores off Baja California (in blue) [*Basak et al.*, 2010]. Coloured vertical bars indicate total variability in measured $\delta^{13}C$ at respective core sites. Coloured circles indicate $\delta^{13}C_{DIC}$ composition of water masses bathing respective core sites under modern conditions [*Key et al.*, 2004].

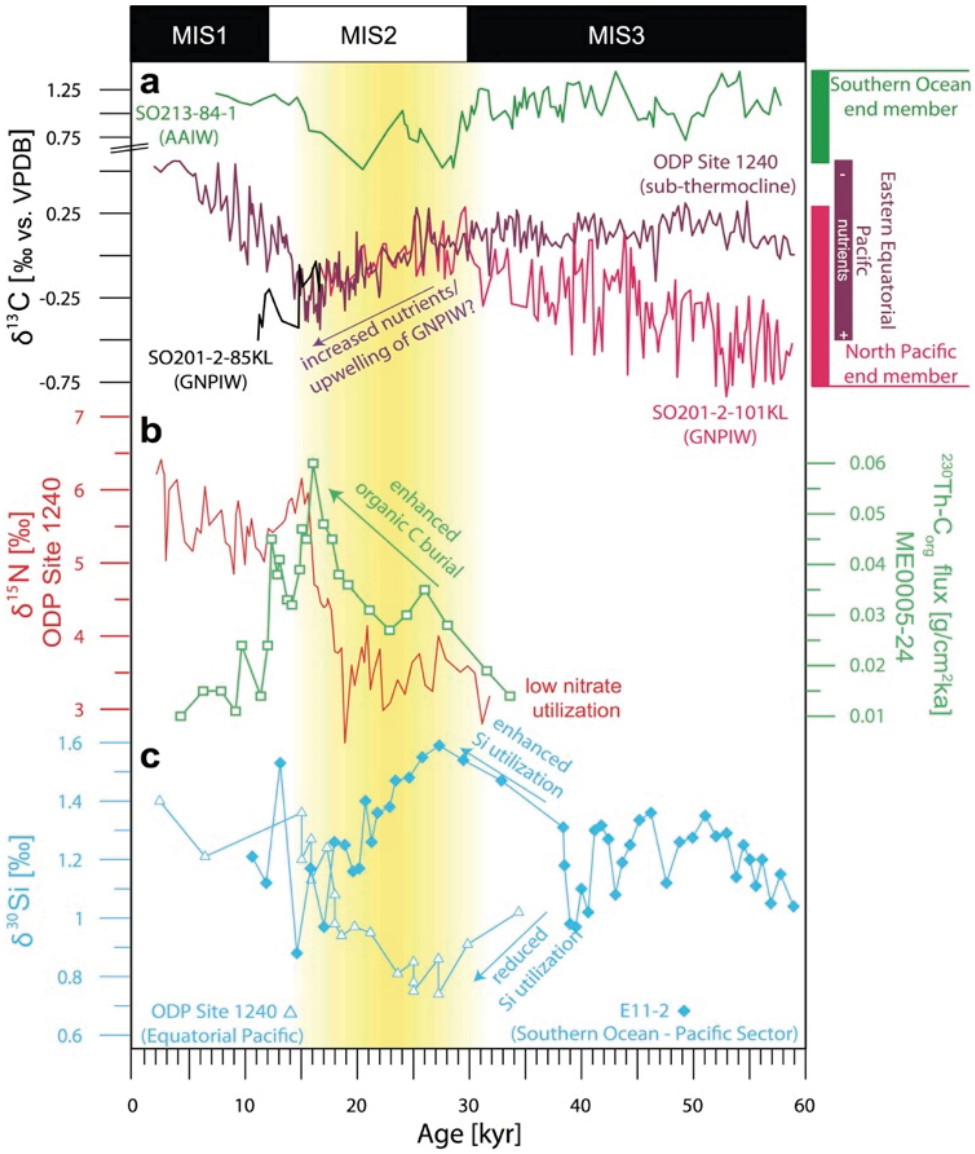

Figure 6 Reconstructed $\delta^{13}C$ variability of GNPIW versus AAIW compared to glacial changes in $\delta^{13}C$ of sub-thermocline waters, biological productivity and nutrient utilization in the Eastern Equatorial Pacific (EEP) and Southern Ocean. a: $\delta^{13}C$ record of GNPIW (SO201-2-85KL, *Max et al.*, 2014; SO201-2-101KL; *this study*) compared to $\delta^{13}C$ composition of AAIW (SO213-84-1, *Ronge et al.*, 2015) and deep-dwelling planktonic foraminifera $\delta^{13}C$ record of *G. hexagonus* (ODP Site 1240, this study) during the past 60 kyr. b: $\delta^{15}N$ record at ODP Site 1240 in the EEP [*Pichevin et al.*, 2009] together with ^{230}Th-normalized C_{org} flux of neighbouring core ME0005-24 [*Kienast et al.*, 2007]. c: $\delta^{30}Si_{Diatom}$ isotope composition of ODP Site 1240 in the EEP [*Pichevin et al.*, 2009] compared to $\delta^{30}Si_{Diatom}$ composition derived from core E11-2 [*Robinson et al.*, 2014] located in the Pacific Zone of the Southern Ocean. Yellow shaded bar marks times of increased GNPIW contribution to sub-thermocline waters of the EEP during MIS 2.